JOURNAL OF MATERIALS SCIENCE 31 (1996) 6195–6200

Fracture toughness of eutectic Al–Si casting alloy with different microstructural features

M. F. HAFIZ
Al-Azhar University, Faculty of Engineering, Department of Mechanical Engineering, Nasr City, Cairo, Egypt

T. KOBAYASHI
Toyohashi University of Technology, Department of Production Systems Engineering, Toyohashi, Aichi 441, Japan

The static fracture toughness of a series of eutectic Al–Si casting alloy with different microstructural features has been evaluated. The dominant influence of eutectic silicon in controlling the fracture toughness is thus clarified. The relationship between the fracture toughness and the microstructure was established. Fracture toughness was found to be strongly associated with the size and morphology of silicon particles. The other feature which greatly influences the fracture toughness is the ratio $(\lambda/DE)_{Si}$, i.e. the silicon particle spacing divided by the equivalent particle diameter, rather than the silicon particle spacing, λ_{Si}. Fracture toughness also correlates well with the void growth parameter, VGP ($= \sigma_y (\lambda/DE)_{Si}$), proposed by the authors. The results of the present work can be used to develop an understanding of the variation of fracture toughness with the microstructural features of eutectic Al–Si alloys.

1. Introduction

Aluminium–silicon (Al–Si) alloys are being used in an ever increasing variety of applications (e.g. automotive and aerospace). These applications generally attempt to take advantage of the higher strength to weight ratio and good thermal and electrical conductivity, as well as excellent casting characteristics. Mechanical properties of these alloys are known to be largely dependent on the eutectic silicon particles characteristics (i.e. size and morphology) as well as the eutectic silicon spacing. A considerable number of studies [1–6] have concentrated on developing an understanding of the tensile properties of Al–Si casting alloys.

Despite the obvious design situation (e.g. aerospace and automotive components) where the fracture toughness would be of great value, efforts to evaluate this property for Al–Si casting alloys are lacking. This singular lack of information available on the fracture toughness of these alloys has restricted their use somewhat unjustifiably to areas where fracture toughness-related properties are not of significant importance. However, the importance of fracture toughness evaluation in Al–Si castings as an important means to improve their capacity to withstand the demands of service conditions, cannot be over-emphasized. Understanding of the microstructural features which control the toughness of Al–Si casting alloys will allow proper materials specifications to be written for those applications where toughness-related failure must be prevented.

The current work was undertaken to establish a framework for understanding the variation of the static fracture toughness of eutectic Al–Si casting alloy with different microstructural features.

2. Experimental procedure

2.1. Material

The eutectic Al–Si alloy used in this study was prepared from high-purity aluminium and silicon. Its chemical composition (mass %) was 12.6Si, 0.001Mn, < 0.01Mg, 0.004Cu, 0.0008P, 0.0002Fe and balance of aluminium. To provide for a variation in the microstructural features, versions of this alloy were treated by different amounts of strontium prior to casting into graphite and steel moulds. Details concerning melting and strontium, as well as casting procedures, are given elsewhere [7].

2.2. Fracture toughness test

Fracture toughness measurements are carried out using an Instron testing machine at 8.3×10^{-3} m ks^{-1} (0.5 mm min^{-1}) crosshead speed, on fatigue pre-cracked three-point bend specimens at room temperature (~288 K). Fig. 1 shows the configuration of the test specimens used. The fatigue pre-crack was produced under the conditions recommended by ASTM [8]. This was achieved by cyclically loading the notched specimens with a load ratio, R ($= P_{max}/P_{min}$) < 0.1. Pre-cracking load was decreased stepwise as

0022–2461

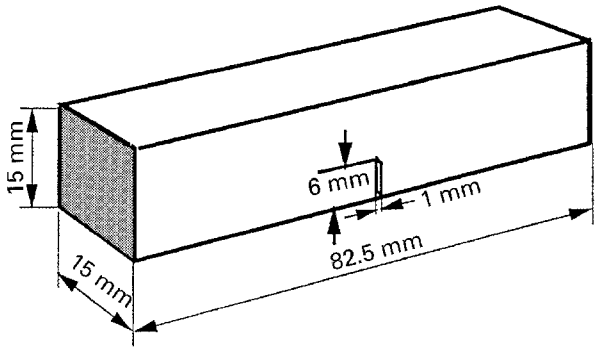

Figure 1 Configuration of three-point bend specimen used in static fracture toughness test.

the fatigue pre-crack advanced in order to keep a low stress intensity factor as suggested by the ASTM standard [8]. The final crack length, a, to the specimen width, W, was kept in the range of 0.5–0.55, for all specimens.

Elastic–plastic fracture toughness characterized by the J-integral concept proposed by Rice [9], as defined by energy rate, was evaluated using the R-curve method [8], which was obtained by the multiple specimen technique. The slope of the blunting line (i.e. $J/\Delta a$) was taken as 2 σ_{flow}, where σ_{flow} is the mean value of the 0.2% proof stress and the ultimate tensile strength. The crack initiation behaviour of the material was characterized by the critical value of J.

2.3. Microstructure

Representative microstructures are shown in Fig. 2. The extremes of the range in silicon size and morphologies found in the present material are clearly observed. Fig. 2a shows the largest silicon particles which were found in unmodified graphite-mould cast alloy. The smallest eutectic silicon is found in 0.024 mass % Sr modified steel-mould cast alloy, which is shown in Fig. 2f. The silicon in the unmodified alloy (Fig. 2a, b) is of plate-like form, while that of the strontium modified alloy (Fig. 2c–f) is of fibrous morphology.

In the present study, the microstructures are quantified by utilizing an image analysis system. The microstructural parameters considered in the present work are the equivalent silicon particle diameter, DE, particle aspect ratio, AR, and shape factor, SF, and the silicon particle spacing, λ_{Si}. These data are reported in Table 1. Definitions and a schematic illustration of these parameters can be found elsewhere [5].

2.4. Fractography

Two approaches have been used in the study of the fracture characteristics of the investigated material. These are examination of the fracture surfaces under the scanning electron microscope (SEM) and observations of the fracture path in relation to the underlying microstructure using an optical microscope. The sequence of events that occur during the fracture mechanics test were also studied on the external surfaces.

3. Results and discussion

3.1. Fracture toughness–microstructure relations

The relationship between the static fracture toughness and the eutectic silicon characteristics is depicted in Fig. 3. This figure shows that the eutectic silicon size and morphology exert a very large effect on the fracture toughness of the present alloy. This dependency can be connected with the difference in the propensity for fracture between the large particles and the smaller ones [10, 11]. This can be rationalized in terms of the stress generated within the elastically deformed particles that conforms with the plastically strained matrix and the size of the flaw likely to be harboured by the fractured particle. These are known to be relatively higher for coarse and slender particles.

The static fracture toughness of the eutectic Al–Si alloy as a function of the eutectic silicon spacing, λ_{Si}, and the silicon particle spacing normalized to silicon particle equivalent diameter, $(\lambda/DE)_{Si}$, is presented in Fig. 4. From this figure, it is very evident that as the interparticle spacing increases static fracture toughness decreases inversely with the ratio $(\lambda/DE)_{Si}$. This type of relationship between the static fracture toughness and λ_{Si} as well as $(\lambda/DE)_{Si}$, is also reported for hypoeutectic Al–Si alloy [5]. These correlations demonstrate that the fracture toughness of Al–Si alloys is greatly controlled by $(\lambda/DE)_{Si}$ rather than λ_{Si}. Hence the trend shown by the latter conflicts with the expectation that increasing the particle spacing provides a better resistance to void coalescence, and thus higher fracture toughness [12, 13].

In Fig. 5 the static fracture toughness of the present alloy is plotted as a function of the void growth parameter, VGP, proposed by the authors [5]. As can be seen, a linear relationship exists between the fracture toughness and VGP. The positive slope of the best line fit reflects the increase in the fracture toughness with an increase in VGP value. On the other hand, the good correlation shown in this figure confirms the significance of VGP in controlling the fracture toughness of the present alloy.

3.2. Fracture characteristics

Fig. 6 documents the stages of the fracture process in the alloy under consideration during the static fracture toughness test. It can be seen that as the external load is applied to a pre-cracked specimen, the tensile stress opens up the crack tip. Then plastic deformation blunts the crack tip, resulting in a stretched zone, while voids begin to form ahead of the crack tip. The stretched zone continues to increase and the void grow, until a critical stretched zone size is reached. Then the crack begins to propagate by linking of the voids with the blunted crack tip (cf. Fig. 6a). The localized plasticity can also be seen in Fig. 6b.

Investigating the crack path in the mid-section using optical microscopy, Fig. 7, suggests that, in the present alloy, three fracture events may be envisaged as occurring almost continuously as the crack advances, i.e. silicon particles progressively enter a plastic zone ahead of the crack tip and progressive void

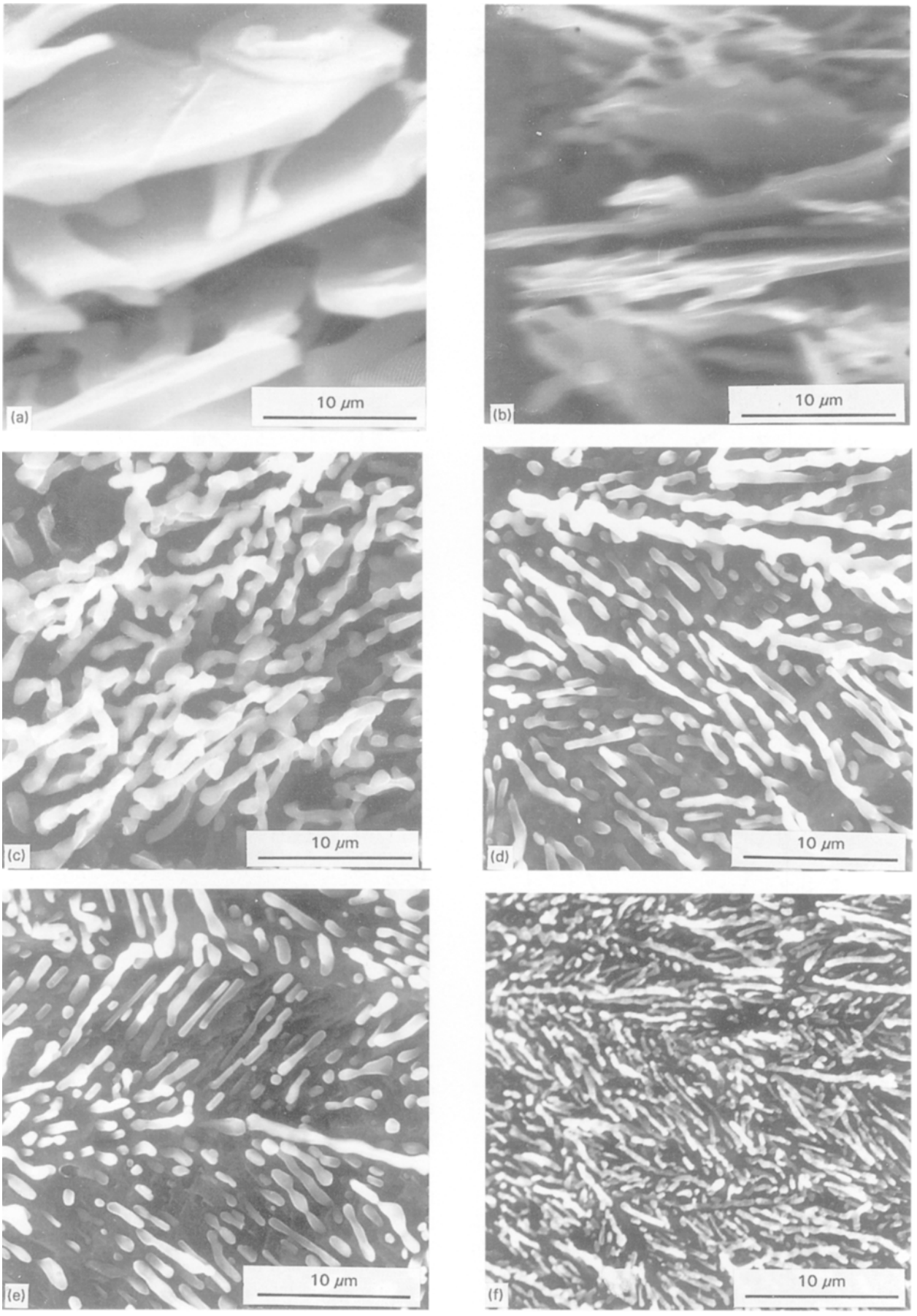

Figure 2 Micrographs depicting the microstructure of eutectic Al–Si alloy. (a, b) Unmodified alloy, (c) 0.0087 Sr, (d) 0.012 Sr, (e) 0.028 Sr, (f) 0.024 Sr (mass %).

TABLE I The microstructural features measured on the eutectic Al–Si alloy used in the present investigation

Mould type	Sr content (mass %)	DE (mm)	AR	SF	λ_{Si} (μm)	$(\lambda/DE)_{Si}$
Graphite	0.0000	9.19	18.37	3.81	6.21	0.68
	0.0087	1.27	2.19	2.17	1.82	1.43
	0.0280	0.73	1.65	1.65	1.63	2.23
Steel	0.0000	5.56	15.86	3.15	4.38	0.79
	0.0087	0.86	1.79	1.95	1.75	2.03
	0.0280	0.59	0.93	1.38	1.14	2.39

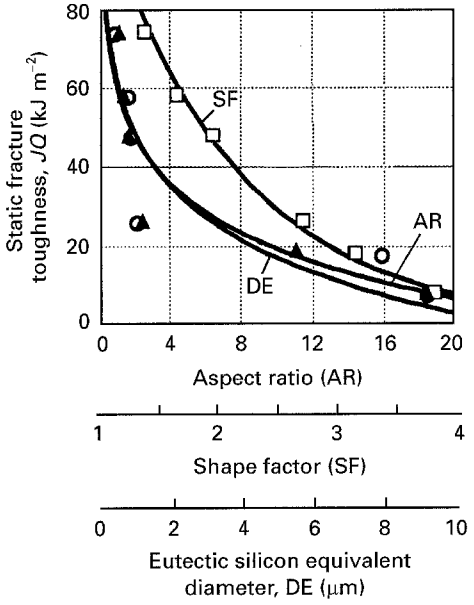

Figure 3 Static fracture toughness as a function of silicon-particle characteristics in eutectic Al–Si alloy: (□) SF, (▲) DE, (○) AR.

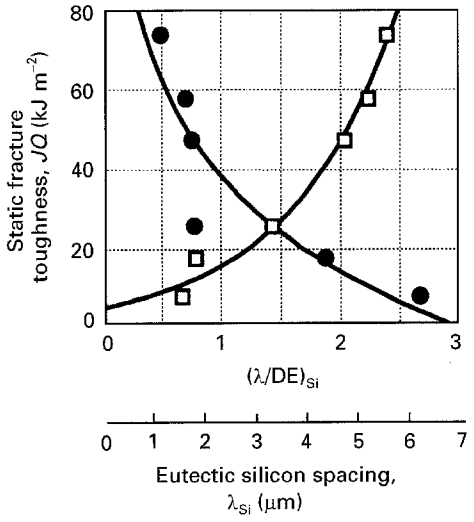

Figure 4 Variation in the static fracture toughness with (●) eutectic silicon spacing and (□) the eutectic silicon spacing divided by the equivalent diameter of a silicon particle.

initiation, growth and coalescence produce increments of crack extension. It is worth noting that the aluminium dendrite caught between the main crack and the submicrocrack appears to be sheared to link up the former with the later. This is likely to occur on further loading.

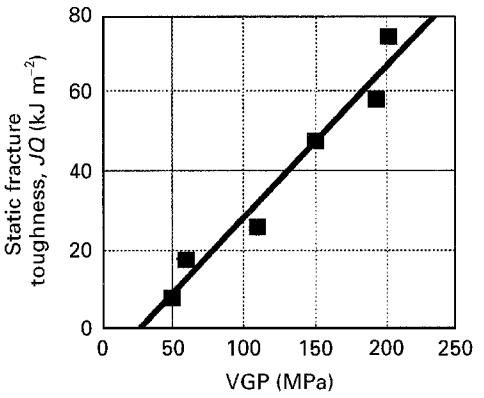

Figure 5 Static fracture toughness versus the void growth parameter VGP. $JQ = -9.94 + 0.38$ VGP. $R'^2 = 0.96$.

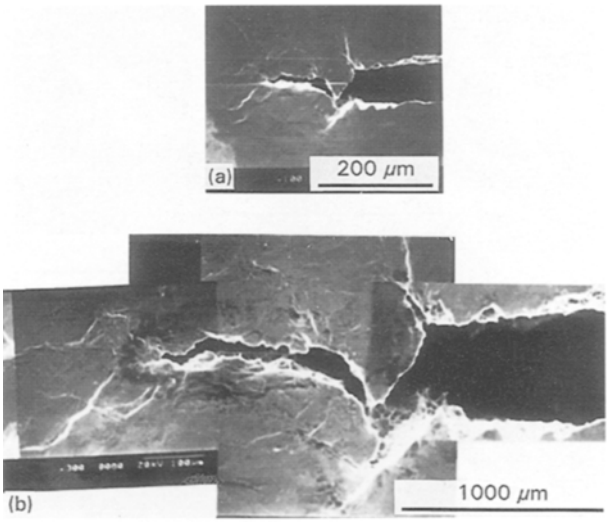

Figure 6 (a) The fracture path during the fracture toughness test, as revealed by SEM on the external surface of the present alloy. (b) Higher magnification of (a).

Combining the external surfaces examination with the mid-plane sections observations, leads to an explanation about the fracture mechanics in the present alloy, as shown schematically in Fig. 8. In this model, it is supposed that, on loading plastic strain in the crack-tip region increases, plastic blunting probably occurs and the crack tip moves forward. At the same time, voids nucleate at the eutectic silicon particles, grow under the influence of the local stress–strain field and the applied stress (i.e. hydrostatic stress). Then these voids either join together or join with the blunted crack tip. However, in the fracture mechanics, initiation is judged to occur when the blunted crack

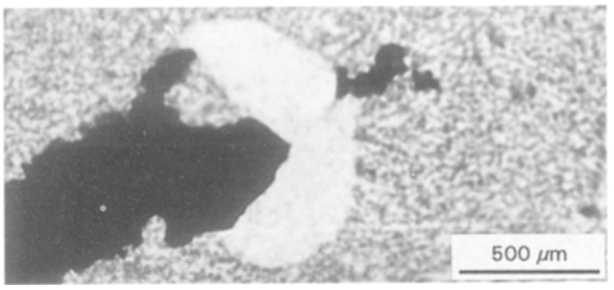

Figure 7 Optical fractograph showing the fracture path in the mid-plane section of 0.024 mass % Sr-modified eutectic Al–Si alloy (steel-mould cast).

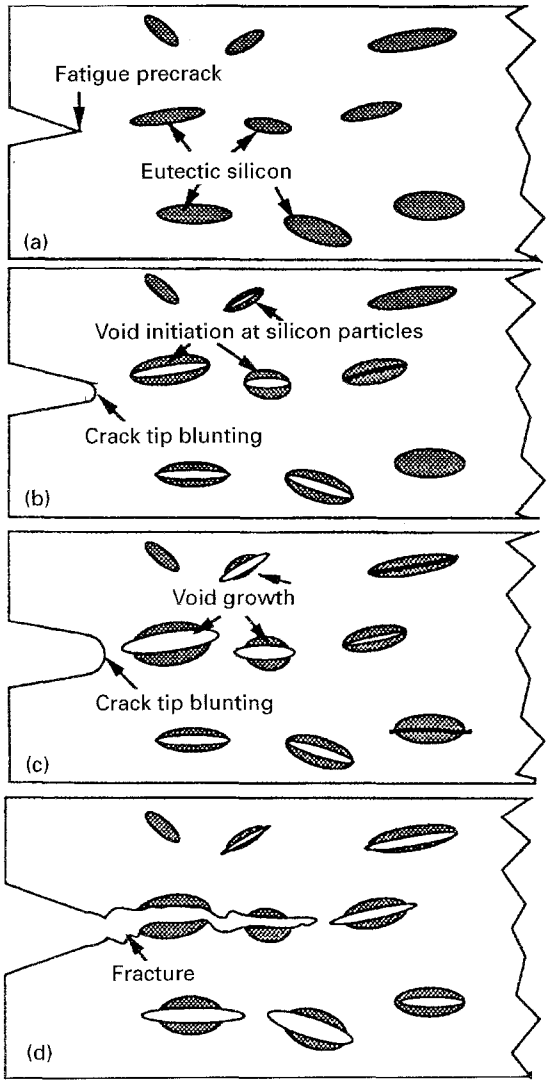

Figure 8 Schematic illustration of the fracture process in the present alloy.

tip links up with the growing void or the expanding microcrack. As a consequence, the fracture energy spent to reach this point is a measure of the fracture toughness. Thus increasing the void initiation resistance and/or decreasing the void growth rate are promising for better fracture toughness in an engineering material. This is likely to be the situation of the present alloy in the modified alloy (i.e. with fine, fibrous silicon morphology and higher VGP).

Fracture surface observations indicated that these stages of fracture proceeded at a low level of deformation in unmodified alloys (characterized by coarse and slender silicon particles), whilst they require a high level of deformation in the modified alloys (with fine and fibrous silicon morphology). The former is judged from the brittle nature of the fracture surfaces of Fig. 9a, b, while the latter can be inferred from the dimple pattern of fracture displayed in Fig. 9c–f. The fractographs of Fig. 9 clearly indicate that the deformation properties of Al–Si alloys are significantly altered by the eutectic silicon particles. The size and morphology, as well as distribution, are important factors controlling the fracture process of these alloys.

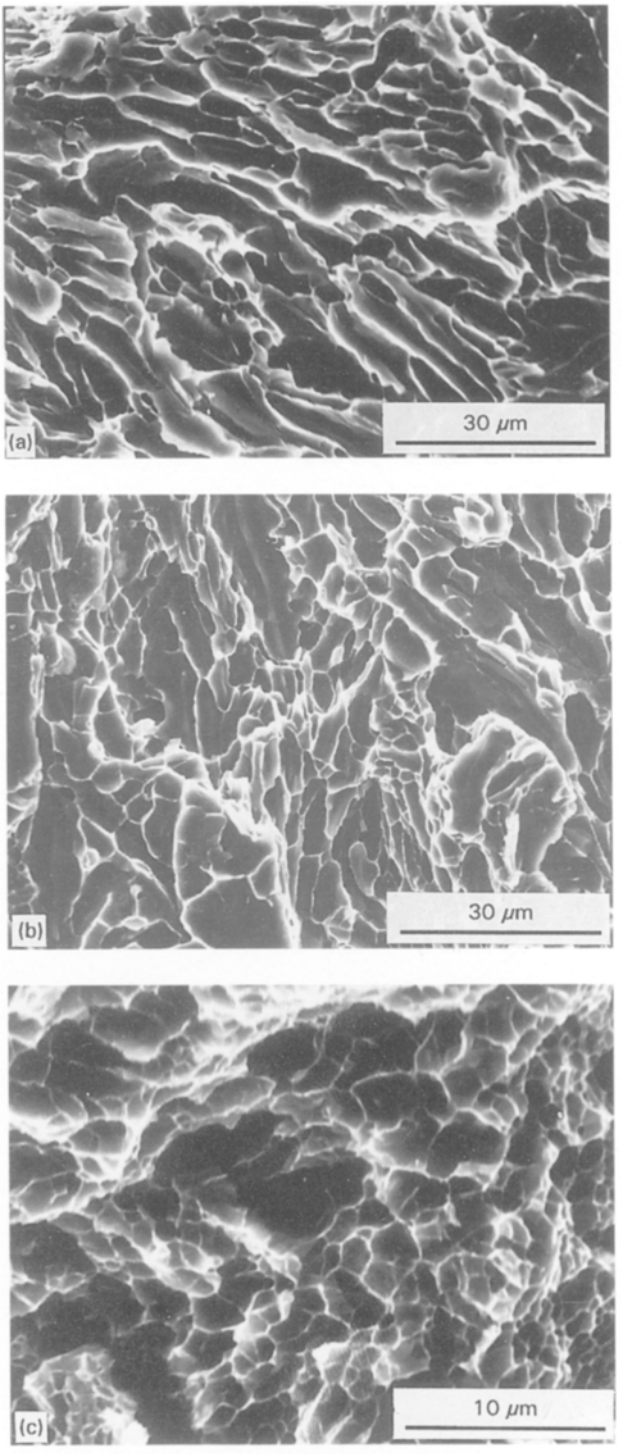

Figure 9 The fracture pattern of eutectic Al–Si alloys broken under static fracture toughness test conditions. (a, b) Unmodified, (c) 0.0087 Sr, (d) 0.012 Sr, (e) 0.028 Sr, (f) 0.024 Sr (mass %). (a, c, e) Graphite-mould cast, (b, d, f) steel-mould cast.

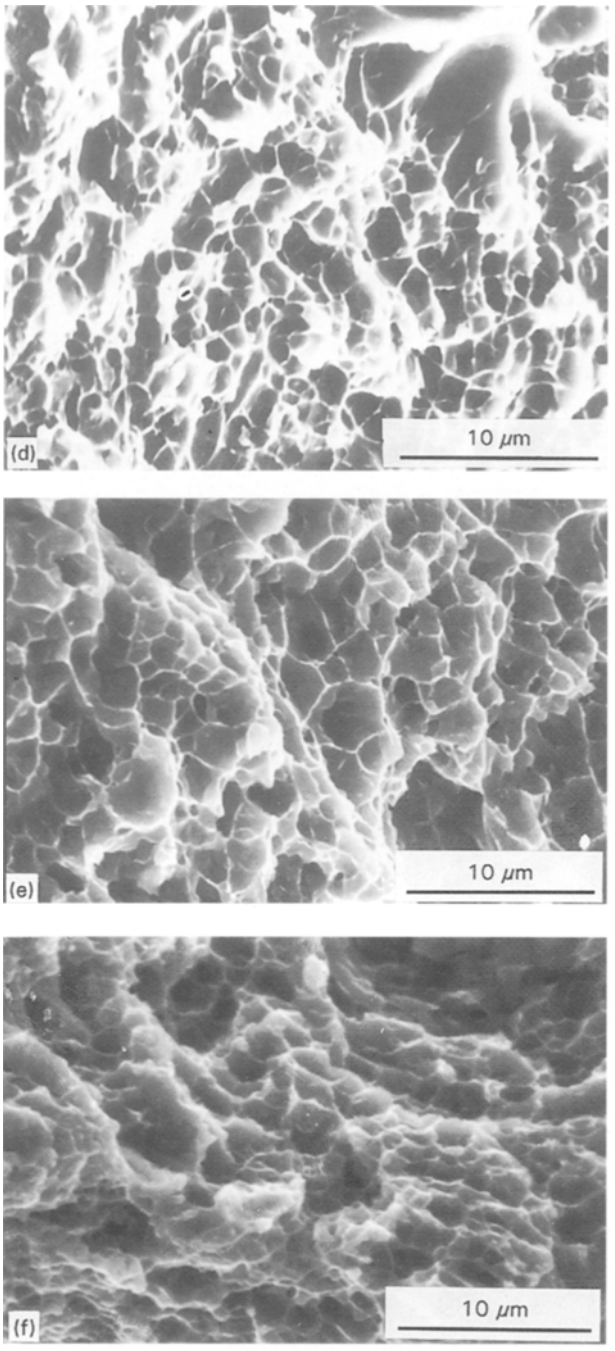

Figure 9 (Continued)

4. Conclusions

Investigating the static fracture toughness of eutectic Al–Si casting alloy with different microstructural features yielded the following conclusions.

1. Decreasing the eutectic silicon spacing coupled with increasing the value of $(\lambda/DE)_{Si}$ has positively affected the static fracture toughness of the present alloy.

2. Decreasing the particle size, DE, by a factor of about 16 and the aspect ratio by a factor of about 20, increases the static fracture toughness by about 77%.

3. The dimple pattern of fracture concomitant with the fibrous morphology of silicon particles suggests that a much higher flow stress is required to attain the required fracture strain, thereby producing higher values of fracture toughness.

References

1. K. J. OSWALT and M. S. MISRA, *AFS Trans.* **88** (1980) 845.
2. S. DAS, A. H YEGNESWARAN and P. K. ROHOTGI, *J. Mater. Sci.* **22** (1987) 3173.
3. K. RADHAKARISHNA, S. SESHAN and M. R. SESHADRI, *AFS Trans.* **88** (1980) 695.
4. A. SAIGAL and K. PRESTON, *ibid.* **96** (1988) 183.
5. M. F. HAFIZ and T. KOBAYASHI, *Scripta Metall. Mater.* **30** (1994) 475.
6. *Idem, ibid.* **31** (1994) 701.
7. M. F. HAFIZ and T. KOBAYASHI, *J. Jpn Inst. Light Metals* **44** (1994) 28.
8. ASTM, "Standard Test Methods for J_{Ic}, a measure of Fracture Toughness", E813-81 (American Society for Testing and Materials, Philadelphia, PA, 1985).
9. J. R. RICE, *J. Appl. Mech.* **35** (1968) 379.
10. A. SAIGAL and J. T. BERRY, *AFS Trans.*, **93** (1985) 699.
11. G. A. ATASOY, F. YILMAZ and ELLIOT, *J. Crystal Growth* **66** (1984) 137.
12. C. W. MEYERS and J. S. LYONS, Technology for Premium Quality *Casting, Metall. Soc.*, edited by E. Dunn and D.R. Durhan, Warrendate PA, 1988, P. 151.
13. G. A. CHADWICK, *Metals Mater.* **20** (1986) 693.

Received 20 September 1995
and accepted 15 January 1996